IEEE Access
Multidisciplinary | Rapid Review | Open Access Journal

Received June 4, 2021, accepted June 28, 2021, date of publication July 6, 2021, date of current version July 13, 2021.

Digital Object Identifier 10.1109/ACCESS.2021.3095081

Humidity Drift Modeling and Compensation of MEMS Gyroscope Based on IAWTD-CSVM-EEMD Algorithms

HUILIANG CAO[1], (Member, IEEE), YUPENG LIU[1], LI LIU[2], AND XINWANG WANG[3]

[1]Science and Technology on Electronic Test and Measurement Laboratory, North University of China, Taiyuan 030051, China
[2]Mechanized Infantry Reconnaissance Department, The Army Infantry Academy of PLA, Shijiazhuang 050083, China
[3]School of Instrument Science and Engineering, Southeast University, Nanjing, Jiangsu 210018, China

Corresponding author: Xinwang Wang (230189684@seu.edu.cn)

This work was supported in part by the National Natural Science Foundation of China under Grant 51705477, in part by the Aeronautical Science Foundation of China under Grant 2019080U0002, in part by the Fund of Key Research and Development (R&D) Projects of Shanxi Province under Grant 202003D111004, and in part by the Fund for Shanxi through the 1331 Project Key Subjects Construction.

ABSTRACT A novel fusion algorithm is proposed based on Improved Adaptive Wavelet Threshold De-noising (IAWTD), C-means Support Vector Machine (CSVM) and Ensemble Empirical Mode Decomposition (EEMD) method to eliminate the humidity drift of MEMS gyroscope. Firstly, the IAWTD method is employed to decrease the humidity drift component in MEMS gyroscope output signal. Then, the humidity drift compensation model is established: the input elements are the relative humidity, the change rate of relative humidity and the humidity drift, and the output is the compensated MEMS gyroscope output signal by EEMD method. In order to verify the compensation effect of the fusion algorithm, the gyroscope outputs are collected and analyzed with the relative humidity ranged from 40% to 90% based on the temperature varying from 20°C to 60°C. The results show that the IAWTD-CSVM-EEMD method significantly reduces the influence of relative humidity drift on the gyroscope output, according to the quantitative analysis of Allan variance, the quantization noise of the gyroscope output decreases by 87.78%, 96.37%, 97.77%, 99.17% and 92.62% respectively under the relative humidity ranging from 40% to 90%, as the temperature rose from 20 °C to 60 °C at intervals of 10 °C. In addition, the bias stability decreases by 96.9%, 99.41%, 99.1%, 99.46%, and 99.78% respectively and the angle random walk decreases by 88.16%, 96.54%, 98.16%, 94.43%, and 92.05% respectively at different temperatures. It is worth mentioning that, to further verify the applicability of the fusion algorithm, a group of comparative experiments are added to consider the influence of temperature changes on the gyroscope output under different relative humidity. The experimental results show that the quantization noise, bias stability and angle random walk of the MEMS gyroscope are significantly reduced compared with the original output after processing by IAWTD-CSVM-EEMD. Therefore, the method proposed in this paper is beneficial to reduce the humidity drift in the MEMS gyroscope output.

INDEX TERMS MEMS gyroscope, relative humidity, humidity drift model, Allan variance.

I. INTRODUCTION

With the development of the MEMS technology, inertial devices including accelerometers and gyroscopes are more and more widely used in inertial navigation. Gyroscopes, as one of the most significant inertial devices, include various types such as MEMS gyroscopes, fiber optic gyroscopes, and laser gyroscopes. Among them, the application of MEMS gyroscopes in military and daily life is particularly important. However, the development of MEMS gyroscopes faced significant technological challenges including large noise, drift and non-linear scale factor, as well as properties vulnerable to temperature and humidity [1]. Many attempts have been made to improve the above deficiencies by studying temperature characteristics of MEMS gyroscopes. Typically, Ma *et al.* [2] proposed a parallel denoising model

The associate editor coordinating the review of this manuscript and approving it for publication was Claudia Raibulet.

based on PE-ITD (Permutation entropy-Intrinsic time-scale decomposition) and SA-ELM(Simulated annealing-Extreme learning machine) in order to solve the temperature drift of MEMS gyroscopes. Result shows that the angular random walk is decreased obviously from 0.0104°/h/p Hz to 2.665 × $10^{-5^{\circ}}$/h/p Hz, and the bias stability improves from0.1874°/h to 1.599 × $10^{-3^{\circ}}$/h with a temperature range from −40° to 60° (enhanced by 99.1%). This method is more accurate and effective. Gu textitet al. [3] conducted experiments based on an improved CEEMDAN (Complete ensemble EMD with adaptive noise)-Bagging ELM compensation method which can enhance generalization performance and boost compensation accuracy of the model, and it was found that the bias instability reduced from 0.0785°/s to 0.0046°/s. Also there are other proposed methods to solve the denoising problems such as Radial basis function neural network (RBF-NN), Back propagation neural network (BP-NN), Kalman filter, Wavelet threshold denoising, Support vector machine (SVM) [4]–[13]. These studies mainly focused on how to reduce the temperature drift of MEMS gyroscopes, however, the detailed influence of humidity on MEMS gyroscopes is still lacking.

Relative humidity has been all part of the most significant factors which affect the performance of MEMS gyroscope. The main component of MEMS gyroscope is made of silicon, which is very sensitive to relative humidity. This unique property is due to the fact that the water vapor may permeate the micro cracks and microspores of MEMS gyroscopes with the condition of high relative humidity, which will restrain the extraordinary precision application of MEMS gyroscopes. On the other hand, the structure of beam adhesion of MEMS inertial devices may be damaged under the condition of high relative humidity. Then the failure of the package might be led to the intrusion of water vapor which caused the changes of capacitance, resistance and other electrical parameters. It may be equally caused the accumulation of adhesion, delamination, electrochemical corrosion, corrosion fatigue and so on.

To decrease the humidity drift of MEMS gyroscopes, many scholars proposed hardware methods. Song *et al.* [14] found that adhesion was a well-known failure mode in micro-electromechanical system, and most of them were influenced by relative humidity. A capacitive MEMS micro-accelerator is studied and analyzed that the capillary force was the theory of adhesion influenced based on accelerator. According to some materials test, it was proved that choosing electrode material with high contact angel and large roughness, as well as processing the contact surface with hydrophobic layers is a better method to decrease adhesion dominated by relative humidity. Aono *et al.* [15] proposed a method which is water-level packaging to reduce the influence of relative humility and found that an environment of high relative humility was constructed to test the performance of the gyroscope. Makkonen *et al.* [16] tested that a 3-axis gyroscope was to be tested under the condition of high relative humidity, and found that the high relative exactly affected the performance of the gyroscope. Patel and Mccluskey [17] also tested a MEMS gyroscope which under the high relative humidity condition, but they did not propose how to reduce the influence of high relative. It can be concluded that the majority of the existing research focused on the high relative humidity, while fewer optimized the structure of the gyroscope to accuracy its performance. In addition, hardware methods spend more time and money, and under this condition, other methods such as software compensation, which are more time-saving and cost saving, needs urgent development.

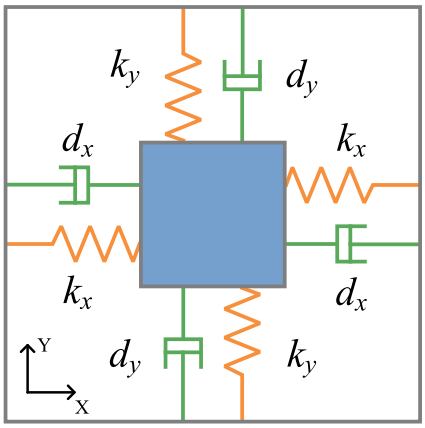

FIGURE 1. The structure of drive and sense mode.

In this paper, first of all, the structure and model of LSM6DS3 MEMS gyroscope is conducted. Secondly An improved method which called IAWTD-EEMD-CSVM(Improved Adaptive Wavelet Threshold De-noising - Ensemble Empirical Mode Decomposition-C-means Support Vector Machine)was proposed to deal with the relative humidity error. Next, the output data of X axis under the ranges of temperature from 20°C to 60°C and the relative humidity from 40%RH to 90%RH is discussed. Finally, The Allan variance analysis method was utilized to compare the performance of the MEMS gyroscope and improve practicability and significance of the suggested methods.

II. THE STRUCTURE AND MODEL OF LSM6DS3 MEMS GYROSCOPE

The structure of the LSM6DS3 gyroscope has two modes, drive mode and sense mode, as shown in Figure 1, which can be assorted into two parts: X-axis drive structure and Y-axis sense structure.

The whole structure can be saved into a spring-mass-damping system. Specifically, When the spring-mass-damping system is working, the drive mode drives the driving mass and the Coriolis mass vibrated linear along the drive axis, when the angular rate input to Z-axis, according to the Coriolis theorem, it will receive the Coriolis force along the sense mode direction based on Y-axis spring-mass-damping system, which will drive the sense mass moves along the sense direction. Y sense axis spring-mass-damping system has the same structure and motion mode. Under

Newton's second law, the product of acceleration and its mass received by the mass is the sum of the external forces. Then the force equation in the driving direction and detection direction is shown in formula (1)[18]:

$$\begin{bmatrix} m_{dx}a_{dx} \\ m_{sy}a_{sy} \end{bmatrix} = \begin{bmatrix} F_{dx} \\ F_{sy} \end{bmatrix} - \begin{bmatrix} F_{kdx} \\ F_{ksy} \end{bmatrix} - \begin{bmatrix} F_{cdx} \\ F_{csy} \end{bmatrix} + \begin{bmatrix} F_{edx} \\ F_{esy} \end{bmatrix} \quad (1)$$

where m_{dx} and m_{sy} represent X axis drive mass and Y axis sense mass, respectively. a_{dx} and a_{sy} represent X axis drive mass acceleration and Y axis sense mass acceleration, respectively. F_d, F_k, F_c, and F_e represent the matrix of electrostatic force, elastic force, damping force, and system external force (such as impact, picking, etc.), respectively. The elastic force and damping force matrix in the Gyroscope structure obtained from Figure 2 can be defined as listed in formula (2).

$$\begin{bmatrix} F_{kdx} \\ F_{cdx} \\ F_{ksy} \\ F_{csy} \end{bmatrix} = \begin{bmatrix} k_{dx} & & & \\ & c_{dx} & & \\ & & k_{sy} & \\ & & & c_{sy} \end{bmatrix} \begin{bmatrix} x \\ x \\ y \\ y \end{bmatrix} \quad (2)$$

where k_{dx} and c_{dx} represent the drive matrix of X axis elastic force equivalent stiffness and damping force equivalent damping, respectively. k_{sy} and c_{sy} represent the sense matrix of Y axis elastic force equivalent stiffness and damping force equivalent damping, respectively. Combining the above formulas, a new matrix of MEMS gyroscope can be established in formula (3).

$$\begin{bmatrix} m_{dx}\ddot{x} \\ m_{sy}\ddot{y} \end{bmatrix} + \begin{bmatrix} c_{dx} & -2m_{dx}\Omega_z \\ 2m_{sy}\Omega_y & c_{sy} \end{bmatrix} \begin{bmatrix} \dot{x} \\ \dot{y} \end{bmatrix} + \begin{bmatrix} k_{dx} - m_{dx}\Omega_z^2 & -m_{dx}\dot{\Omega}_z \\ m_{sy}\dot{\Omega}_z & k_{sy} - m_{sy}\Omega_z^2 \end{bmatrix} \begin{bmatrix} x \\ y \end{bmatrix} = \begin{bmatrix} F_{dx} \\ F_{sy} \end{bmatrix} \quad (3)$$

where Ω_z represents input angular velocity. And then the motion of MEMS gyroscope can be described according to these above formulas as illustrated in the formula (4).

$$\begin{cases} m_{dx}\ddot{x} + c_{dx}\dot{x} + k_{dx}x = F_{dx} \\ m_{sy}\ddot{y} + c_{sy}\dot{y} + k_{sy}y = -2m\Omega_z y \end{cases} \quad (4)$$

The circuit structure of the gyroscope is divided to drive mode part and sense mode part as shown in Figure 2. The drive mode part is an AGC-PLL closed loop including the gyroscope structure of drive mode, amplification factor, 90° shifter, rectifier, low-pass filter, adder, multiplier, and constant DC power supply. Different from the drive mode part, the sense mode part is a sense open loop including the gyroscope structure of sense mode, amplification factor, low-pass filter, and multiplier.

According to the drive mode closed loop, a weak signal which produced by the structure of drive mode is called V_{dx}, this signal is so weak that need to amplify. The signal passes through the signal amplifier to obtain the amplified signal V_{damp}, and then the signal V_{damp} is sent to the 90° shifter to obtain a quadrature signal V_{dl} that is different from the signal V_{dx}. The signal V_{dl} is divided into two channels. One is sent to the rectifier and low- pass filter to extract the amplitude part of the signal and filter out the excess noise, the other is

TABLE 1. The circuit factors of drive mode.

w_{dx}	Resonance frequency
Q_x	Quality factor
K_{ampx}	Amplification factor of the forward
b_x	A factor of low-pass filter
λ_x	A factor of low-pass filter
V_{dc}	A constant DC voltage

TABLE 2. The circuit factors of sense mode.

w_{dy}	Resonance frequency
Q_y	Quality factor
K_{ampy}	Amplification factor of the forward channel
b_y	A factor of low-pass filter
λ_y	A factor of low-pass filter
V_{out}	An output DC voltage
Ω_z	An input angular velocity

sent to the multiplier. After these processes, the signal $|V_{dl}|$ is sent to the adder, and the signal generated by the adder is distinguished to obtain signal V_{da}. The signal V_{da} multiplied with another signal V_{dl} produces the modulated signal V_{dll}, and the signal V_{dll} overlaid with a DC signal V_{dc} produces a complete AC signal. The complete AC signal is fed back and finally sent to the drive mode structure of the gyroscope.

The input angular velocity is converted into the driving force of the sense mode and acts on the sense mode structure of the gyroscope when entering the gyroscope structure of gyroscope from the Z axis due to the Coriolis force.

After processing the Coriolis force by the sense mechanical structure, a weak voltage signal V_{sy} is output at the sense output terminal of the gyroscope. The voltage signal V_{sy} is firstly amplified by the forward channel amplifier, and then modulated with the reference signal of the driving mode. With the obtained modulated signal V_{sl} is obtained, the signal V_{sl} is filtered through a low-pass filter to get the final signal V_{out}. According to the formula (5), the output angular velocity of the gyroscope can be calculated.

$$\Omega_z = \frac{V_{out}}{K} \quad (5)$$

where Ω_z represents the output angular velocity and K represents the scale factor.

III. ALGORITHMS AND MODEL

A. ENSEMBLE EMPIRICAL MODE DECOMPOSITION (EEMD)

The empirical study shows that there are still some defects in the use of Empirical Mode Decomposition (EMD) model because the EMD method assumes that the time series analyzed is not affected by noise, and the Intrinsic modal function (IMF) component obtained by decomposition can reflect

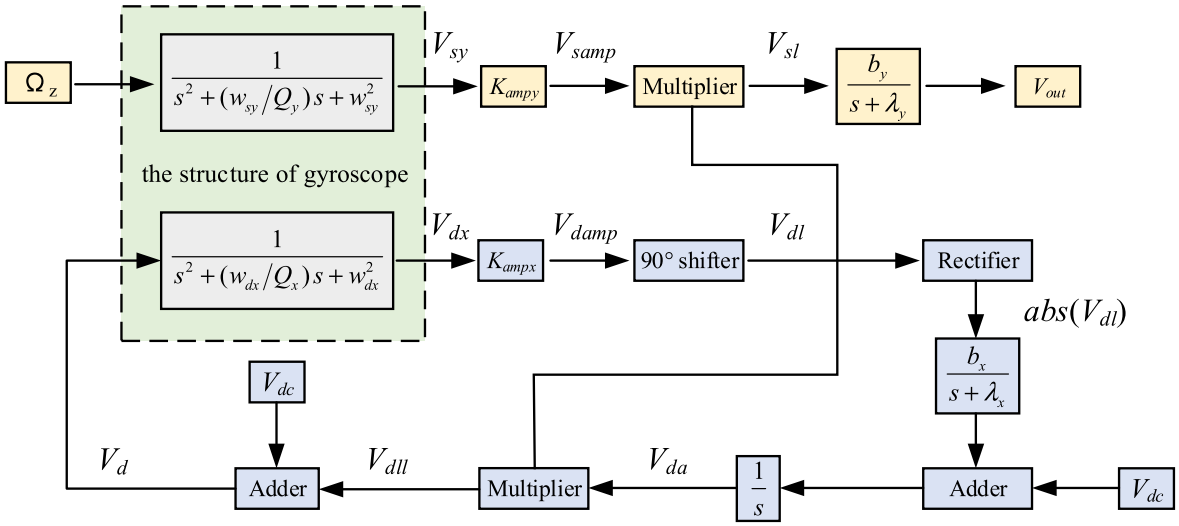

FIGURE 2. The circuit structure of the gyroscope.

the characteristics of the original time series. However, in real life, there must be noise in the actual acquired time series, especially when the amount of data is large, and the existence of noise is inevitable. Therefore, the phenomenon of modal mixing will occur, which means that the classification of signal components does not correspond to IMF components, that is, there may be multiple signal components containing the same IMF component. Scales of these signal components are different, and there may also be signal components of the same scale that appear in multiple IMF components. The phenomenon of mode aliasing in EMD affects the decomposition effect. To alleviate the mode aliasing, Wu and Huang added white noise to assist the decomposition and proposed the Ensemble Empirical Mode Decomposition (EEMD) model.

When the poles of the signal to be decomposed are not uniformly distributed or the signal has local disturbances, EMD decomposition will cause defects such as modal aliasing and end effects, resulting in multi-component composite signals that cannot separate the components of the signal. In response to the uneven distribution of poles that may appear in the original signal, EEMD uses the uniform distribution of each frequency in the white noise spectrum to mix the white noise with the original signal to improve the uneven distribution of the poles of the original signal. In order to eliminate the interference of white noise on the original signal, the EEMD algorithm uses the characteristic that the amplitude of is zero, and performs EMD decomposition by adding multiple sets of white noise, and then calculates the average of multiple sets of decomposition results to eliminate the impact of auxiliary white noise on the decomposition results. Statistically speaking, the more the white noise is added, the smaller the influence of auxiliary white noise on the decomposition result. The steps of the EEMD algorithm are as follow [19]–[21]:

1) Determine the number of overall averages M, add the white noise group $n_j(t)$,(j $= 1, \ldots, M$),to the original signal $x(t)$, and the composite signal mixed with noise is expressed as $x'(t)$.

2) Find all the extreme points of $x'(t)$, and the minimum points are connected to constitute the lower envelope $E_l(t)$, and the connection between the maximum points constitutes the upper envelope $E_u(t)$. The, the center line $e_m(t)$ of these two envelopes can be expressed as the formula (7):

$$e_1(t) = \frac{E_u(t) + E_l(t)}{2} \tag{6}$$

3) Subtract the mean of the envelopes from the signal $x'(t)$, calculate the difference between $x'(t)$ and $e_1(t)$ and obtain $h_1^1(t)$:

$$h_1^1(t) = x'(t) - e_1(t) \tag{7}$$

4) Iterative screening is performed on $h_1^1(t)$, and the intrinsic mode function $h_1^{k1}(t)$ satisfying the formula (8) is obtained, where ε is the threshold value for EMD to stop iterative screening.

$$\left(\sum \left[h_1^k(t) - h_1^{k+1}(t)\right]^2\right) / \sum \left[h_1^k(t)\right]^2 \leq \varepsilon \tag{8}$$

5) Subtract $h_1^{k1}(t)$ from the original signal $x(t)$ to get the residual r_2:

$$r_2(t) = x(t) - h_1^{k1}(t) \tag{9}$$

6) Take r_2 as the new signal $x'(t)$ to be decomposed, and repeat steps 2) to 5) to get the new intrinsic mode function $h_1^{k2}(t)$ and the new residual component r_3.

7) Repeat Step 6) to obtain n intrinsic mode functions $h_1^{ki}(t)$, $i = 1, 2, \ldots$,n and the residual r_{n+1}. In order to facilitate reading, $h_1^{ki}(t)$ is rewritten as $h_i(t)$.

$$r_{n+1}(t) = x'(t) - \sum_{i=1}^{n} h_i^{k_i}(t) \tag{10}$$

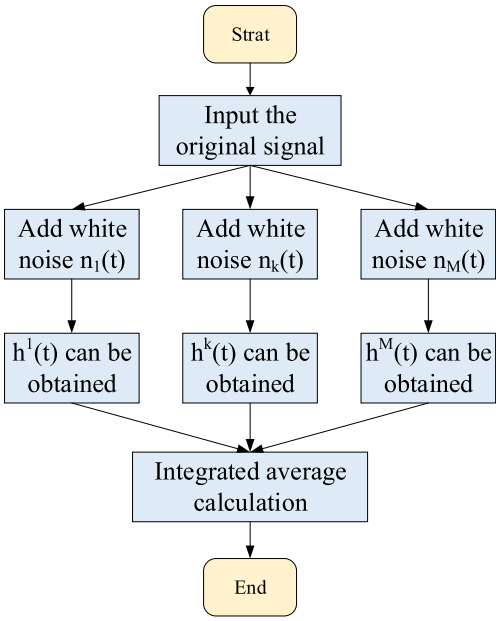

FIGURE 3. The process of EEMD.

8) Stop EMD decomposition until r_{n+1} is a monotonic function or constant value.

9) Repeat the operation from step 2) to step 8) M times, the different white noise sequence is added to complete the EMD decomposition at each time, then the $h_i^j(t)$ can be obtained, where j is the number of white noise additions.

10) Finally, the white noise interference is eliminated through the formula (11), and each IMF of the EEMD can be obtained.

$$IMF_i = [\sum_{j=1}^{M} h_i^j(t)]/M \tag{11}$$

The algorithm flow of EEMD is shown in Figure 3.

B. WAVELET THRESHOLD DE-NOISING (WTD)

The Wavelet Threshold De-noising (WTD) mainly consists of the following three steps:

1) The orthogonal wavelet transform of noisy signal is calculated. Based on the noisy signal whose length is n and $n = 2^J$, the fast algorithm of orthogonal wavelet transform can be used to obtain the scale coefficients in low resolution $\{v_{L,K}, k = 1, 2, 4 \ldots, 2^L\}$ and the wavelet coefficients $\{w_{j,k}, j = L, L+1 \ldots, J-1, k = 1, 2, 4, \ldots, 2^j\}$ in each resolution, including scale coefficients and wavelet coefficients. The periodic extension method is often used when dealing with boundaries.

2) The wavelet coefficients are processed by non-linear threshold. In order to keep the overall shape of the signal unchanged, all low-frequency coefficients $\{v_{L,K}, k = 1, 2, 4 \ldots, 2^L\}$ are reserved. Before processing the wavelet coefficients, the wavelet threshold value and the wavelet threshold function need to be determined. Commonly-used threshold estimation methods include fixed threshold estimation, maximum and minimum threshold estimation, heuristic threshold estimation and unbiased risk estimation, etc. In this paper, unbiased likelihood estimation applicable to high-frequency components is selected to determine the threshold. Take the absolute value of each element in signal $y(i)$ and sort it by size, then square each element to get the new signal $f(k)$:

$$f(k) = (sort(|y|))^2, \quad k = 0, 1, \ldots, N-1 \tag{12}$$

If the square root of the kth element of $f(k)$ is taken as the threshold λ_k, that is:

$$\lambda_k = \sqrt{f(k)} \tag{13}$$

The risk generated by this threshold is:

$$risk(k) = \frac{N - 2k + \sum_{i=1}^{k} f(j) + (N-k)f(N-k)}{N} \tag{14}$$

According to the obtained risk curve *risk(k)*, the position corresponding to its minimum risk point is denoted as k_{min}, then the unbiased risk estimation threshold is:

$$\lambda = \sqrt{f(k_{\min})} \tag{15}$$

After obtaining the threshold, the soft threshold, hard threshold, and soft-hard threshold are used to process each wavelet coefficient.

3) The wavelet transform is carried out. All the low-frequency scale coefficients, as well as the wavelet coefficients after threshold processing, is reconstructed by inverse wavelet transform in order to get the estimated value of the original signal.

The soft threshold, hard threshold, and soft-hard threshold are three different functions, which are displayed in formulas (16), (17), and (18), respectively. In Equation (18), the parameters p and q are regulatory factors to obtain a suitable threshold function.

$$\bar{w}_{j,k} = \begin{cases} w_{j,k} & |w_{j,k}| \geq \lambda \\ 0 & |w_{j,k}| < \lambda \end{cases} \tag{16}$$

$$\bar{w}_{j,k} = \begin{cases} sign(w_{j,k} - \lambda) & |w_{j,k}| \geq \lambda \\ 0 & |w_{j,k}| < \lambda \end{cases} \tag{17}$$

$$\bar{w}_{j,k} = \begin{cases} sign(w_{j,k}) \left[|w_{j,k}| - \frac{p\lambda}{q^{|w_{j,k}-\lambda|}+c-1} \right] & |w_{j,k}| \geq \lambda \\ 0 & |w_{j,k}| < \lambda \end{cases} \tag{18}$$

According to practical engineering and previous experience, soft threshold and hard threshold functions have certain disadvantages. The hard threshold function only retains most of the wavelet coefficients, but takes another small part of

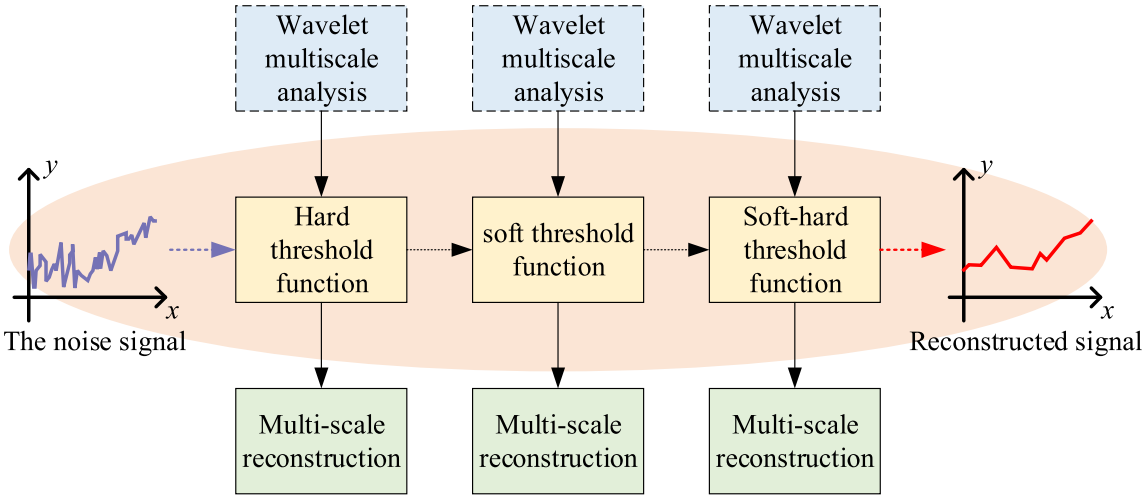

FIGURE 4. The steps of WTD method.

the coefficients directly to zero, resulting in a discontinuity at the threshold position of the filtered coefficients, which will cause the signal oscillation in the reconstruction process, while the soft threshold function takes most of the coefficients. The wavelet coefficients use the reduction transformation, which will not affect its discontinuity, but the filtered coefficients have a certain deviation λ between $\bar{w}_{j,k}$ and $|w_{j,k}|$, which will change the approximation between the reconstructed signal and the original signal.

In summary, the steps of Wavelet threshold de-noising method are shown in Figure 4. Wavelet threshold de-noising method can not only eliminate the noise basically, but also retain the useful signal as much as possible to ensure the integrity and feature points of the signal, so it has good de-noising effect which it can be applied for different types of a complex signal.

C. THE IMPROVED ADAPTIVE WAVELET THRESHOLD DENOISING BASED ON HUMIDITY

According to the soft-hard threshold function, which is shown in formula (18) and the relative humidity and characteristic of MEMS gyroscope, the threshold function of traditional wavelet threshold denoising method is improved, and the new improved adaptive threshold function is proposed in this paper.

In an un-damped or slightly damped (vacuum or air) environment, the microbeam of MEMS gyroscope can be equivalent to an ideal spring mass model, from which the theoretical equation of the resonance frequency of the microbeam can be derived as:

$$w_0 = \frac{K}{M} = \frac{Ybh^3}{4L^3M} = \frac{Ybh^3}{4nL^3m_1} \tag{19}$$

where ω_0, M, Y, b, h, L are the resonant frequency, effective mass, Young's modulus, width, thickness, and length of the microbeam. K is the equivalent elastic modulus of the microcantilever; m_1 is the actual mass of microbeam; n is the mass correction factor.

Take the derivation of both sides of equation (19), then the equation (20) can be obtained:

$$\Delta w = -\frac{1}{2}\frac{Ybh^3}{4L^3M^3}\Delta M = -\frac{w_0}{2M}\Delta M \tag{20}$$

So it can be seen that the change of the resonant frequency of the microbeam is proportional to the change of its effective mass.

The relative humidity (*RH*) is defined as the percentage of the actual water vapor pressure E in the environment and the saturated water vapor pressure E at the same temperature. For the MEMS gyroscope, the moisture absorbed by the surface of the microbeam varies linearly with the relative humidity of the environment increasing under certain conditions of its shape, material, and ambient temperature.

In air, the relationship between water film thickness on the surface of the microbeam and the relative humidity is:

$$a/t^3 = (\rho kT/m)\ln RH^{-1} \tag{21}$$

where t is the thickness of the water film; ρ is the density of water; k is the Boltzmann constant Number; T is the thermodynamic temperature; m is the mass of a single water molecule; a is the energy coefficient, $a = 210{*}10^{-19}J$.

And the mass of trace surface water molecules is described as:

$$\Delta m = St\rho = S^3\frac{am\rho^2}{kTRH^{-1}} \tag{22}$$

It can be obtained from equation (21) and equation (22).

$$\Delta m = -\frac{Sw_0^3}{2M}\frac{am\rho^2}{kT^3}\frac{1}{\ln RH^{-1}} \tag{23}$$

where Δm is determined by the shape and size of the microbeam and the temperature is constant and can be

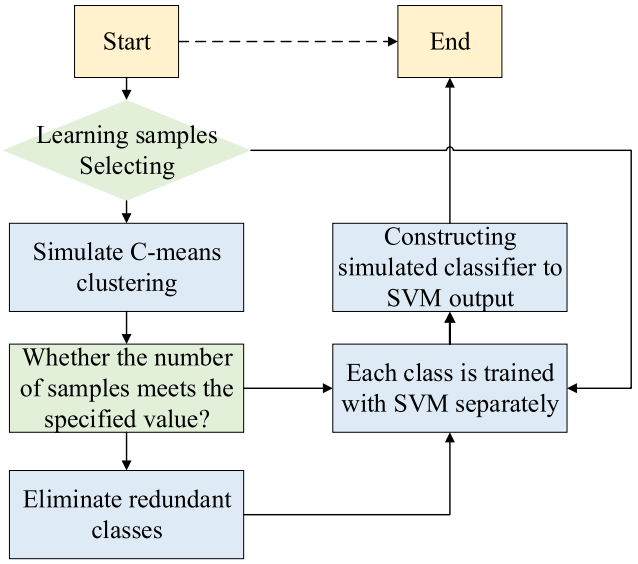

FIGURE 5. The steps of C-SVM algorithm.

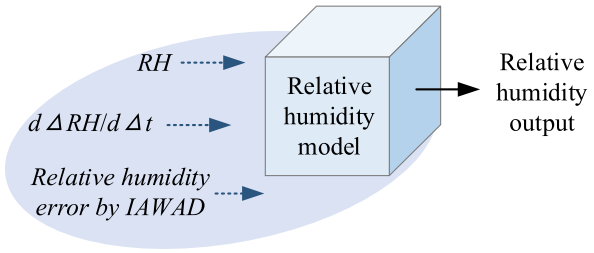

FIGURE 6. The construction of relative humidity model.

regarded as a constant C_0 in this case, so the equation (24) can be obtained:

$$\Delta w = C_0 - \frac{1}{{}^3\ln RH^{-1}} \tag{24}$$

With the increase of the humidity, the resonant frequency of the micro-cantilever beam shifts relative to the original resonant frequency, and the frequency variation is approximately linear with *RH*. Therefore, the relationship equation can be described as:

$$w = -\frac{C_0}{{}^3\ln RH^{-1}} + \mathrm{w}_0 \tag{25}$$

According to the previous literature, there is a certain linear relationship between the output of MEMS gyroscope and the resonance frequency, so based on equation (18) and equation (25), the improved adaptive threshold function can be easily obtained, which is described as:

$$\bar{w}_{j,k} = \begin{cases} sign(w_{j,k})\left[|w_{j,k}| - \frac{C(-\frac{C_0}{{}^3\ln RH^{-1}}+\mathrm{w}_0)\lambda}{d^{|w_{j,k}-\lambda|}+C(-\frac{C_0}{{}^3\ln RH^{-1}}+\mathrm{w}_0)-1}\right] \\ \qquad |w_{j,k}| \geq \lambda \\ 0 \qquad |w_{j,k}| < \lambda \end{cases} \tag{26}$$

where C is the coefficient of MEMS gyroscope.

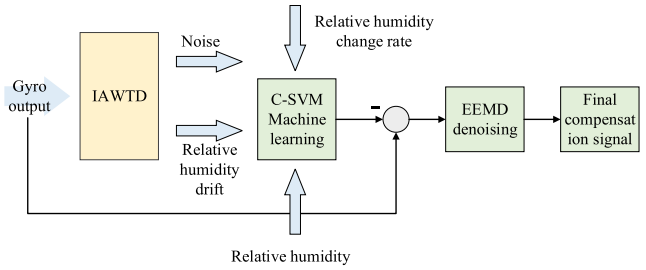

FIGURE 7. The flow chart of EEMD-IAWTD-SVM de-noising method.

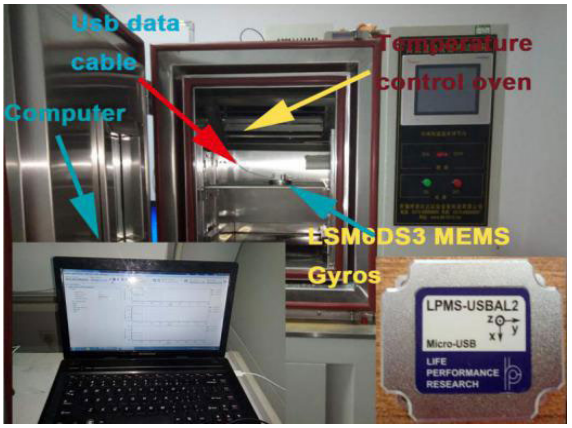

FIGURE 8. The environment of humidity experiment based on LSM6DS3 MEMS gyroscopes.

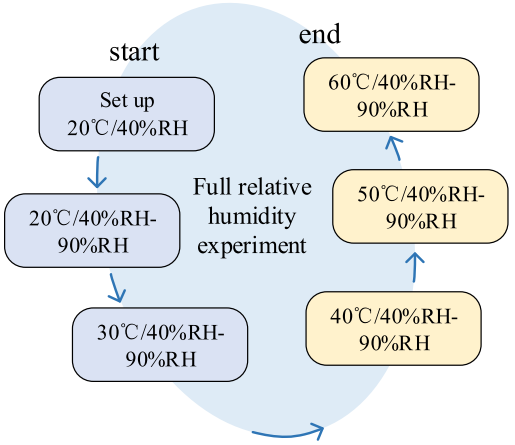

FIGURE 9. The process of full relative humidity experiment.

D. THE IMPROVED SUPPORT VECTOR MACHINE BASED ON FUZZY C-MEANS CLUSTERING

An improved support vector machine algorithm based on fuzzy C-means clustering is proposed to compensate the drift more effectively. The support vector machine algorithm based on fuzzy C-means clustering includes five steps. The steps of C-SVM method are shown in Figure 5.

The C-SVM method is divided into five steps:

(1) Judge whether pre-clustering is needed according to the size of learning sample data. When the number of clusters is

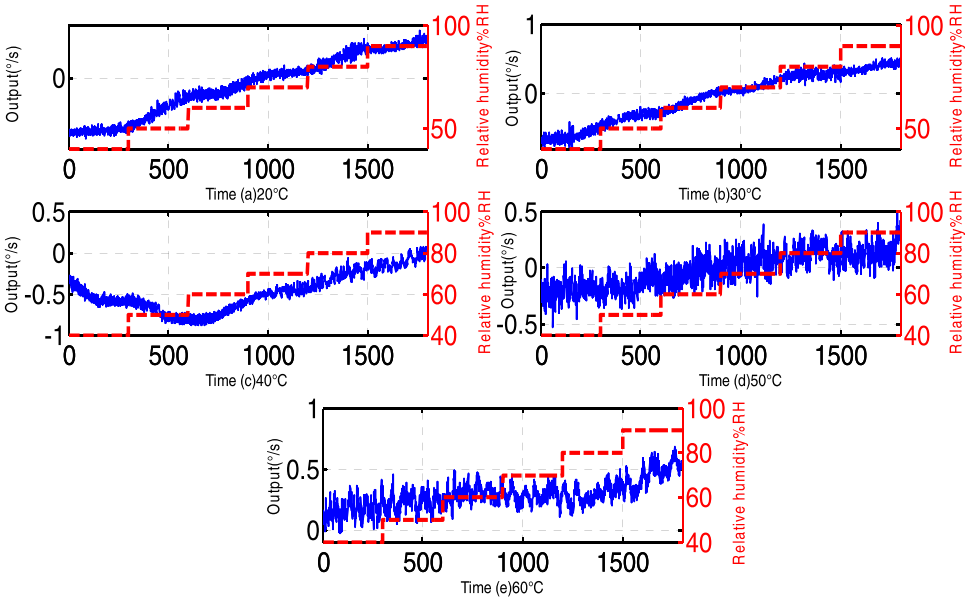

FIGURE 10. The output data under the condition of constant temperature with the relative humidity from 40%RH to 90%RH.

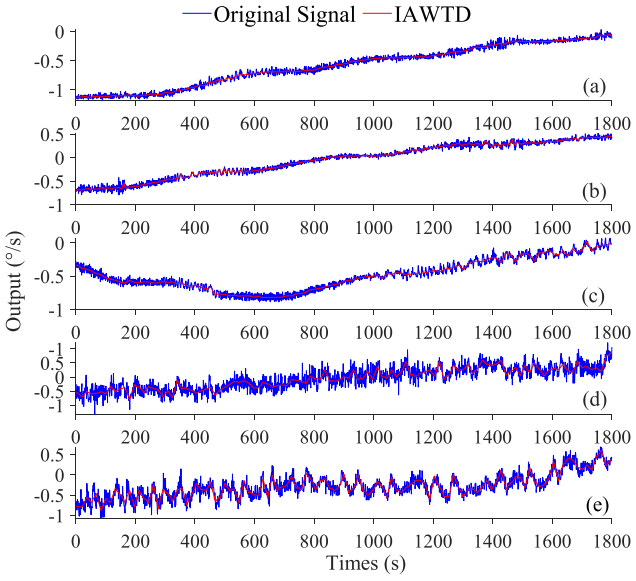

FIGURE 11. The IAWTD curve under the condition of constant temperature with the relative humidity from 40%RH to 90%RH: (a)40% to 90% based on 20°C, (b)40% to 90% based on 30°C, (c)40% to 90% based on 30°C, (d)40% to 90% based on 50°C, and (e) 40% to 90% based on 60°C.

greater than the set value, the number of clusters is calculated and fuzzy c-means clustering is performed.

(2) For each sample, find out the maximum membership degree of each cluster center and classify it into corresponding classes.

(3) After clustering, calculate the number of samples in each class. If the number is less than the corresponding value, the associated class center and the number of redundant classes are eliminated. According to the new clustering number, the samples are clustered again.

(4) Different support vector machines are used to learn different classes.

(5) A fuzzy classifier is constructed to get the output of SVM. The input for each membership degree of sub-SVM is determined, and the output of each sub-SVM model is synthesized according to the membership degree with the final output listed in the formula (27).

$$Y = \sum_{i=1}^{c} u_i Y_i \tag{27}$$

where C is the number of classes, Y_i is the output of the first i support vector machine, and u_i is the test sample points to the membership degree of each cluster center. u_i is related to the square of the distance from the sample point to the cluster centers. It can slightly ensure that the SVM of similar classes plays a greater role in the output of classification synthesis.

$$u_i = \begin{cases} 1 & d\,(x, c_i) \neq 0 \\ \dfrac{1/d^2(x,c_i)}{\sum_{j=1}^{c} 1/d^2(x,c_j)} & d\,(x, c_j) \neq 0 \end{cases} \tag{28}$$

where $d(x,c_i)$ expresses the euclidean distance between the input and the corresponding clustering center, and c_i expresses the center of class i.

E. CONSTRUCTION OF RELATIVE HUMIDITY MODEL

In order to eliminate the relative humidity error, it is very important to establish a high-precision relative humidity compensation model. Therefore, the humidity drift compensation model based on the improved adaptive wavelet threshold denoising (IAWTD) and C-SVM is proposed. It is worth mentioning that this compensation model is a multi-input/single-output model, which can improve the learning

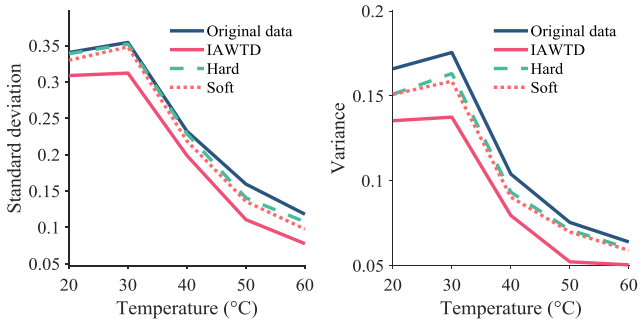

FIGURE 12. The comparison of standard deviation and variance based on original data, hard, soft and IAWTD.

and prediction ability of the model and thus further improve the compensation effect of the hybrid algorithm. The relative humidity model is shown in Figure 6, for a group of training data obtained in advance, the relative humidity, the relative humidity change rate and the relative humidity error extracted through IAWTD are taken as the input of the model, and the output of MEMS gyroscope under different relative humidity is taken as the output of the model for training using C-SVM. After the model has been trained, it is used to predict the results generated by the relative humidity in the experimental signal output for the following compensation processing.

F. IAWTD-CSVM-EEMD METHOD

In this paper, the threshold function of wavelet threshold denoising is improved to get the improved adaptive wavelet threshold denoising (IAWTD) method, and the IAWTD-EEMD-CSVM method is obtained by using C-means to improve support vector machine and combining with EEMD denoising algorithm. Figure 7 describes the specific process of IAWTD-CSVM-EEMD method:

(1) By the improved adaptive wavelet threshold denoising (IAWTD), the relative humidity drift in the output signal of gyroscope is extracted.

(2) The C-SVM prediction model is trained in advance, relative humidity, relative humidity change rate and relative humidity drift extracted by IAWTD are taken as the input of the model, and then the model output is subtracted from the original gyroscope output signal to obtain the compensation signal.

(3) After the compensation signal is obtained, it is decomposed into a series of IMFs by EEMD method. After removing the high-frequency IMFs, the remaining IMFs are reconstructed to obtain the final gyroscope output signal.

IV. VERIFICATION AND ANALYSIS

A. EXPERIMENT OF HUMIDITY BASED ON LSM6DS3 MEMS GYROSCOPE

The MEMS gyroscopes were kept on the temperature-controlled oven (Figure 8), free from the outside temperature and humidity variation, with the ranges of relative humidity and relative humidity rate set as 40%RH∼90%RH and

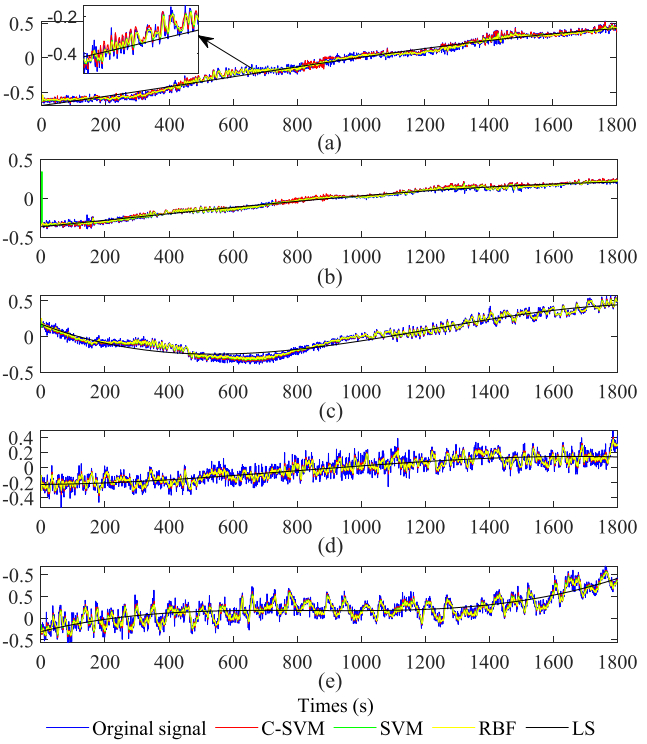

FIGURE 13. The construction of relative humidity model based on C-SVM, SVM, RBF and LS method: (a) 40% to 90% based on 20°C, (b) 40% to 90% based on 30°C, (c) 40% to 90% based on 30°C, (d) 40% to 90% based on 50°C, and (e) 40% to 90% based on 60°C.

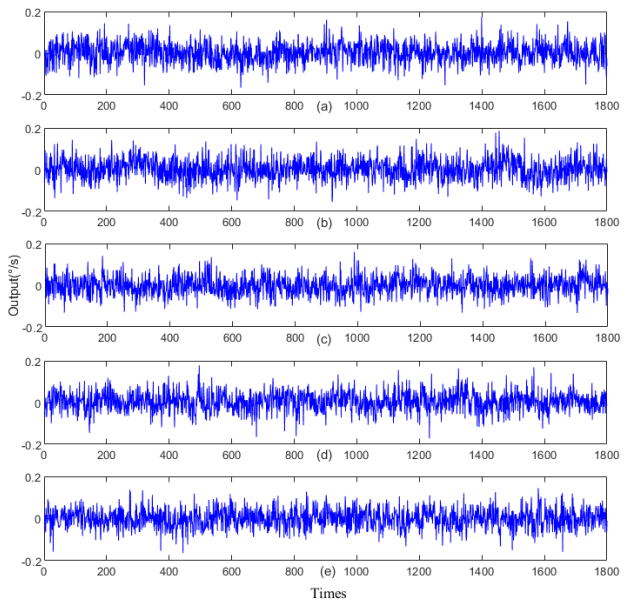

FIGURE 14. The output of MEMS gyroscope after construct the relative humidity model: (a) 40% to 90% based on 20°C, (b) 40% to 90% based on 30°C, (c) 40% to 90% based on 30°C, (d) 40% to 90% based on 50°C, and (e) 40% to 90% based on 60°C.

0.1% RH/min, and then the signal of MEMS gyroscopes was output. The process of the full relative humidity experiment was explained comprehensively as shown in Figure 9.

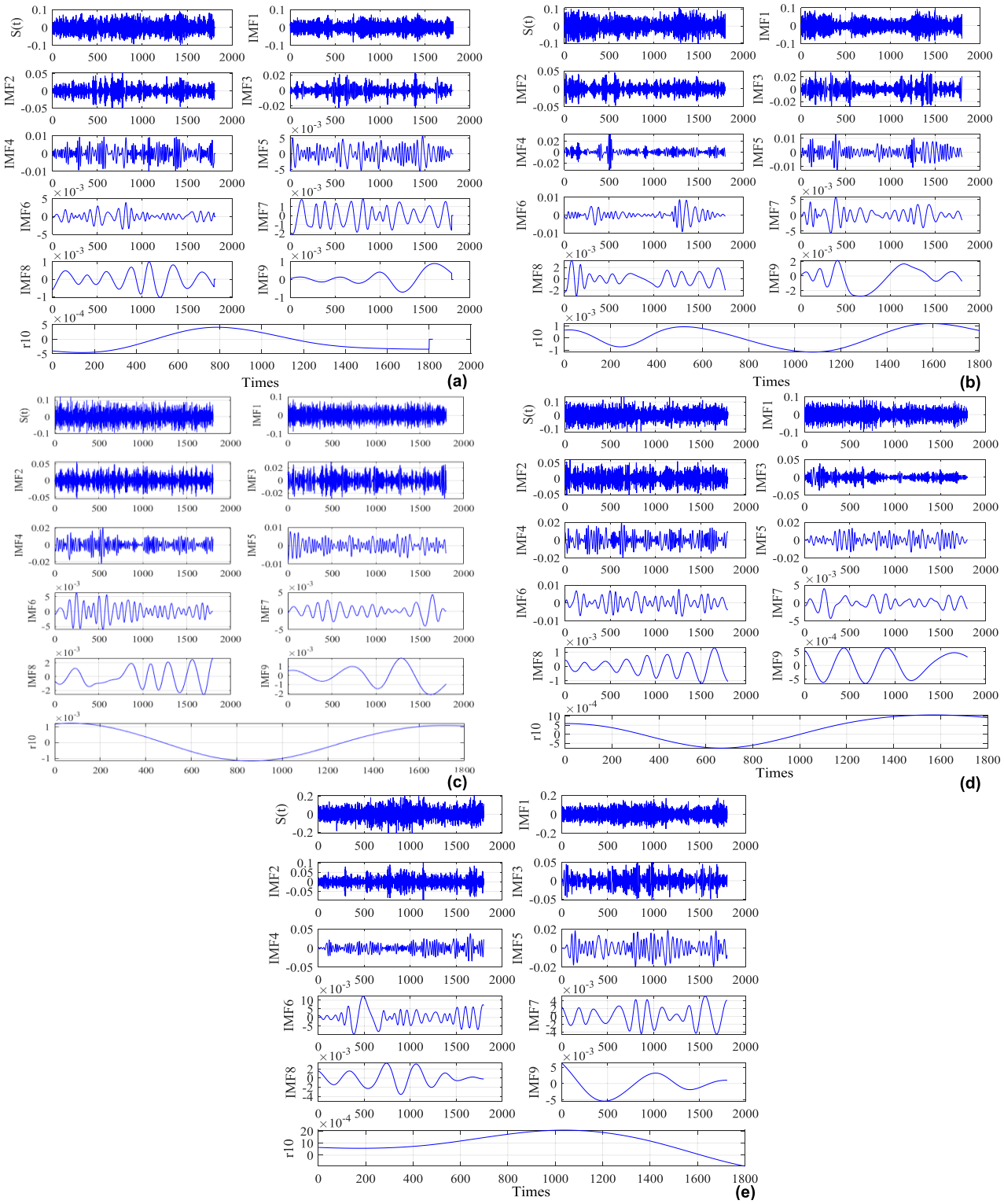

FIGURE 15. The IMFs and residual of EEMD method:(a) 40RH%-90RH% based on 20°C;(b) 40RH%-90RH% based on 30°C;(c) 40RH%-90RH% based on 40°C;(d) 40RH%-90RH% based on 50°C;(e) 40RH%-90RH% based on 60°C.

Firstly, the initial temperature and relative humidity were kept at 20°C and 40%RH for an hour to ensure the stable inside factors. Secondly, the relative humidity was increased to 0.1%RH/min with the temperature remained unchanged. Next, the temperature-controlled oven stayed for an hour every 10% RH to collect the output of the MEMS gyroscopes.

TABLE 3. The comparison of Allan variance based on original signal and IAWTD-CSVM-EEMD.

Temperature	Original signal (°/s)			IAWTD-CSVM-EEMD(°/s)		
	Q	B	N	Q	B	N
20°C	9.66E-04	0.0171	1.47E-04	1.18E-04	0.00052	1.74E-05
30°C	0.0011	0.024	1.66E-04	3.99E-05	0.00014	5.73E-06
40°C	9.63E-04	0.0299	1.57E-04	2.14E-05	2.47E-04	2.88E-06
50°C	0.0032	0.0391	8.41E-05	2.65E-05	0.00021	4.68E-06
60°C	0.0016	0.084	2.19E-04	1.18E-04	0.00018	1.74E-05

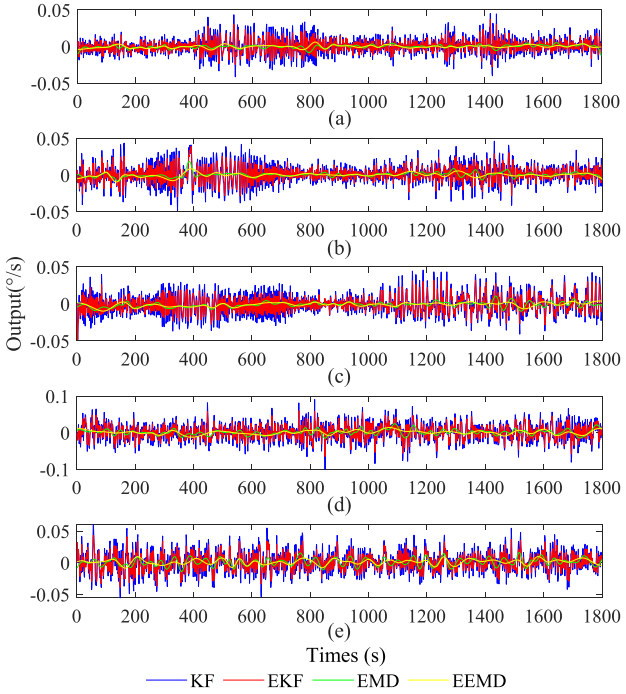

FIGURE 16. The de-noising output based on KF,EKF, EMD and EEMD method: (a) relative humidity 40% to 90% based on 20°C, (b) relative humidity 40% to 90% based on 30°C, (c) relative humidity 40% to 90% based on 40°C, (d) relative humidity 40% to 90% based on 50°C, (e) relative humidity 40% to 90% based on 60°C.

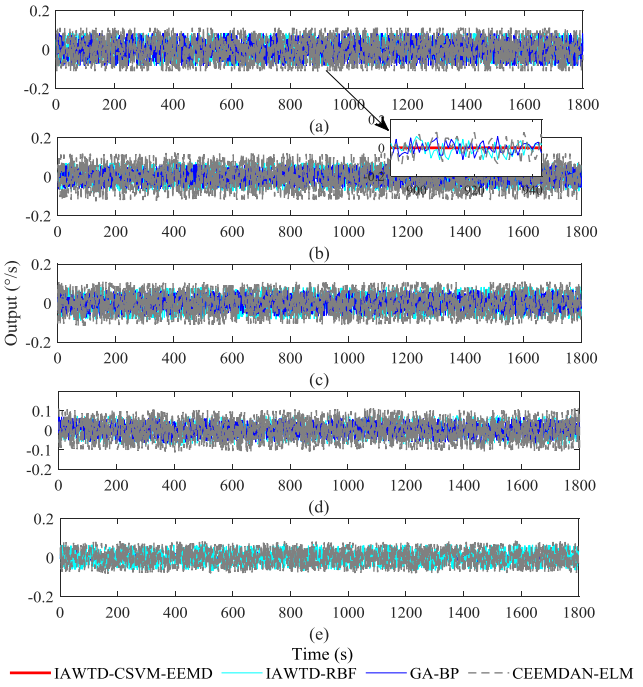

FIGURE 17. The compensation results based on IAWTD-C-SVM-EEMD, IAWTD-RBF, GA-BP and CEEMDAN-ELM method: (a) relative humidity 40% to 90% based on 20°C, (b) relative humidity 40% to 90% based on 30, (c) relative humidity 40% to 90% based on 40°C, (d) relative humidity 40% to 90% based on 50°C, (e) relative humidity 40% to 90% based on 60°C.

Finally, the above process was repeated at temperatures of 30°C, 40°C, 50°C, 60°C, respectively [22]–[25].

Figure 10 displays that the output data with the constant temperature and varying relative humidity (40%RH∼ 90%RH) changed a lot. Therefore, the condition of constant temperature and the relative humidity ranging from 40%RH to 90%RH should be paid more attention to.

B. ANALYSIS OF EXPERIMENTAL RESULTS

According to the steps of the IAWTD-EEMD-CSVM method, first of all, IAWTD is used to denoise the original signal to extract humidity drift. For the purpose of proving the effectiveness of the new method, the traditional wavelet threshold de-noising methods based on soft-threshold function and hard-threshold function are used as the comparative methods.

As shown in Figure 11, the denoising signal waveform became smoother with higher signal reconstruction accuracy and retained useful information after denoising by IAWTD. The variances and standard deviations of wavelet threshold denoising methods based on three threshold functions (soft-threshold function, hard-threshold function, and the improved adaptive threshold function) are shown in Figure 12. After de-noising with the traditional threshold functions, both soft-threshold function and hard-threshold function changed little compared with the variance and standard deviation of the original data. The signal denoised by IAWTD is quite different from the above two methods with the variance and standard deviation reduced compared with the original data. The results show that the relative humidity drift can be well extracted by using the IAWTD method as the input of the relative humidity model.

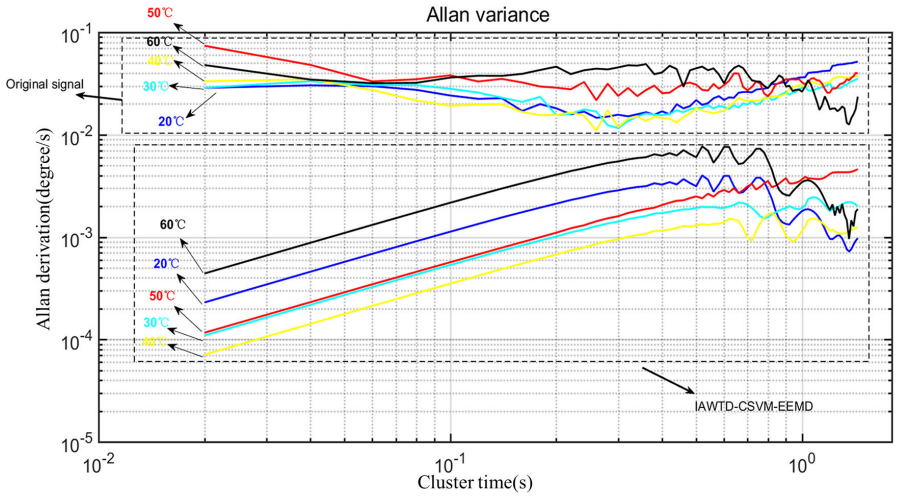

FIGURE 18. The Allan variance curve of original signal and IAWTD-CSVM-EEMD method based on the relative humidity experiment.

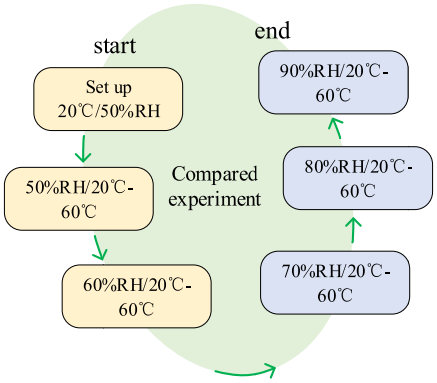

FIGURE 19. The process of compared experiment.

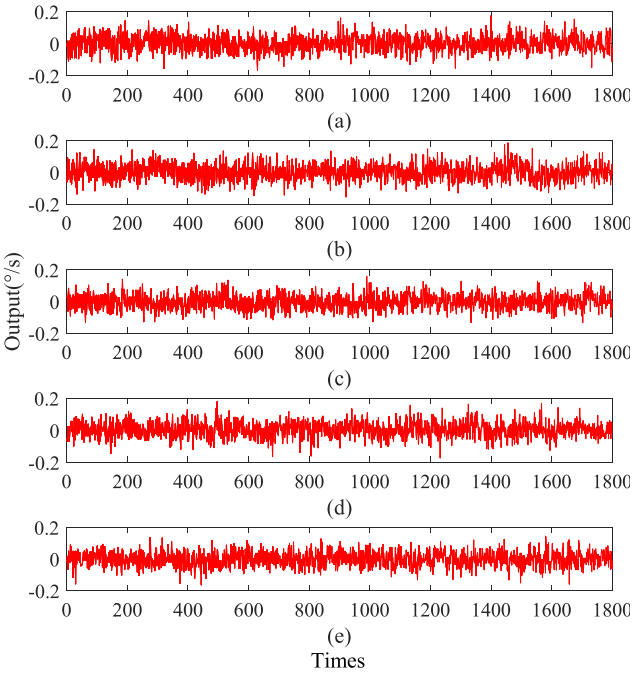

FIGURE 20. Output under the condition with the temperature from 20°C to 60°C: (a) relative humidity 20°C to 60°C based on 50RH%, (b) relative humidity 20°C to 60°C based on 60RH%, (c) relative humidity 20°C to 60°C based on 70RH%, (d) relative humidity 20°C to 60°C based on 80RH%, (e) relative humidity 20°C to 60°C based on 90RH%.

Secondly, the relative humidity model is established using the C-SVM method by taking the relative humidity, the relative humidity change rate and the relative humidity drift extracted from IAWTD as the model input and the original gyroscope output signal as the model output. In order to verify the accuracy of the C-SVM model, this paper compared the relative humidity models established based on the LS method, RBF method, and SVM method. The results are shown in Figure 13. It can be concluded that the relative humidity model established based on C-SVM can better track the original output of the gyroscope. And the compensation output of the C-SVM relative humidity model is shown in Figure 14.

Then, EEMD method is used to denoise the compensated outputs to get the final gyroscope output signals. The decomposition result of EEMD is shown in Figure 15.

To verify the denoising effect of EEMD, three classical methods, KF, EKF and EMD, are used in this paper to compare with EEMD denoising. As can be seen from Figure 16, after the denoising of EEMD, the output of MEMS gyroscope is more stable, the curve is smoother and the relative humidity error is greatly reduced.

After analyzing and comparing the respective performance of IAWTD, C-SVM and EEMD in turn, in order to further verify the compensation effect of IAWTD-C-SVM-EEMD, the results are compared it with IAWTD-RBF, GA-BP and CEEMDAN-ELM [8], [26], [27], the comparison results are given in Figure 17, and it can be seen that IAWTD-C-SVM-EEMD has the best effect.

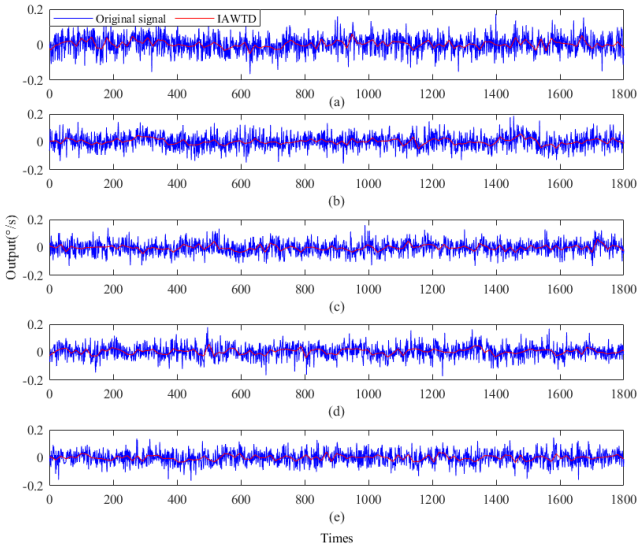

FIGURE 21. The IAWTD curve under the condition of constant humidity with the ranged temperature: (a) relative humidity 20°C to 60°C based on 50RH%, (b) relative humidity 20°C to 60°C based on 60RH%, (c) relative humidity 20°C to 60°C based on 70RH%, (d) relative humidity 20°C to 60°C based on 80RH%, (e) relative humidity 20°C to 60°C based on 90RH%.

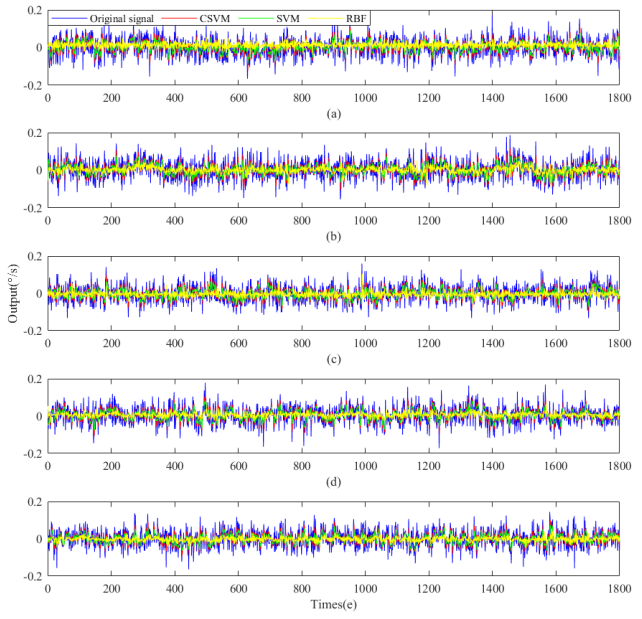

FIGURE 22. The construction of relative humidity model based on C-SVM, SVM, RBF and LS methods under the condition of compared experiment: (a) relative humidity 20°C to 60°C based on 50RH%, (b) relative humidity 20°C to 60°C based on 60RH%, (c) relative humidity 20°C to 60°C based on 70RH%, (d) relative humidity 20°C to 60°C based on 80RH%, (e) relative humidity 20°C to 60°C based on 90RH%.

Allan variance analysis is a method which can evaluate the performance of different types gyroscopes such as MEMS gyroscope, Fiber optic gyroscope, Laser gyroscopes. In order to quantitatively analyze the effect of the method proposed in this paper, Allan variance analysis method is suggested to evaluate compensation effect of gyroscope output in this paper. The Quantization noise (Q), Bias Instability (B) and angle random walk (N) are the most significant factors to

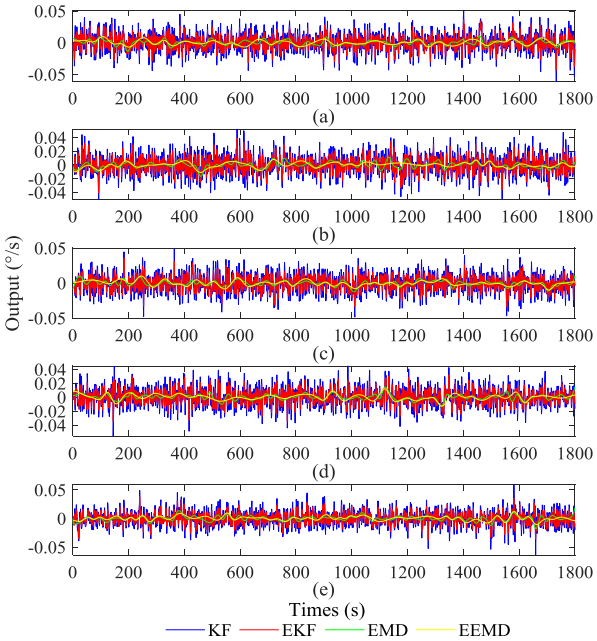

FIGURE 23. The de-noising output based on KF, EKF, EMD and EEMD method: (a) relative humidity 20°C to 60°C based on 50RH%, (b) relative humidity 20°C to 60°C based on 60RH%, (c) relative humidity 20°C to 60°C based on 70RH%, (d) relative humidity 20°C to 60°C based on 80RH%, (e) relative humidity 20°C to 60°C based on 90RH%.

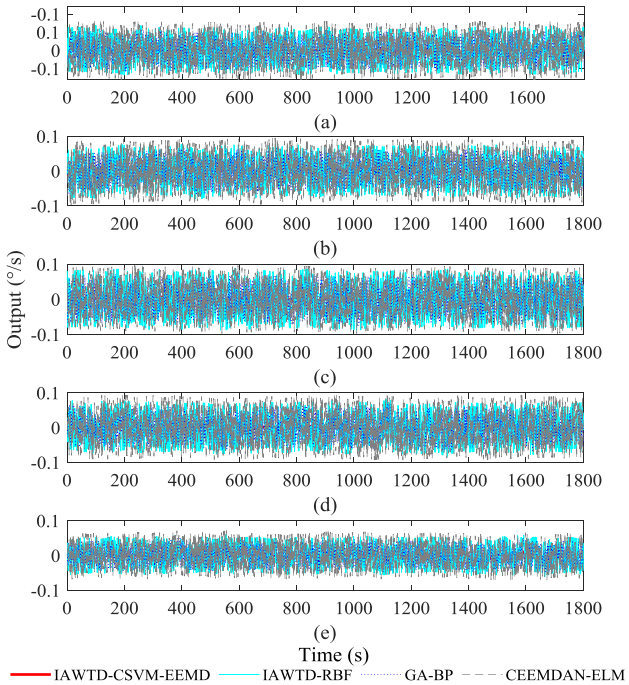

FIGURE 24. The compensation results based on IAWTD-C-SVM-EEMD, IAWTD-RBF, GA-BP and CEEMDAN-ELM method: (a) relative humidity 20°C to 60°C based on 50RH%, (b) relative humidity 20°C to 60°C based on 60RH%, (c) relative humidity 20°C to 60°C based on 70RH%, (d) relative humidity 20°C to 60°C based on 80RH%, (e) relative humidity 20°C to 60°C based on 90RH%.

evaluate the performance. Therefore, the Allan variance curve of original signal and IAWTD-CSVM-EEMD method based on the relative humidity experiment is shown in Figure 18,

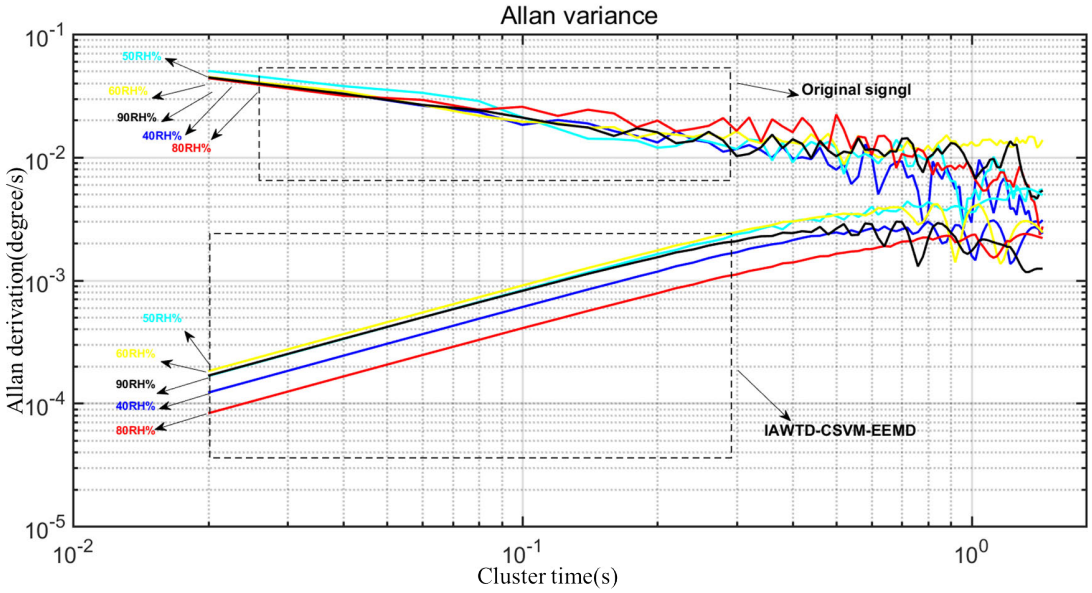

FIGURE 25. The Allan variance curve of original signal and IAWTD-CSVM-EEMD method based on the relative humidity experiment.

TABLE 4. The Allan variance of compared experiment based on original signal and IAWTD-CSVM-EEMD method.

RH	Original signal (°/s)			IAWTD-CSVM-EEMD(°/s)		
	Q	B	N	Q	B	N
50RH	3.09E-04	0.0051	1.12E-04	4.41E-05	8.78E-04	6.01E-06
60RH	6.30E-04	0.0257	1.50E-04	7.02E-05	0.0026	1.01E-05
70RH	2.77E-04	0.0069	1.13E-04	6.73E-05	0.0017	9.32E-06
80RH	4.27E-04	0.0313	7.22E-05	2.12E-05	0.0017	3.77E-06
90RH	3.74E-04	0.0132	1.18E-04	6.18E-05	0.0024	8.97E-06

the factors of Q, B, N based original data and IAWTD-CSVM-EEMD method are shown in Table 3.

By using IAWTD-CSVM-EEMD method, the outputs of MEMS gyroscope which were ranged from 40% relative humidity to 90% relative humidity based on the temperature from 20°C to 60°C respectively is reduced, the relative humidity drift was reduced a lot. For example, the factor of Q is reduced from 9.66E-04 to 1.18E-04 at 20°C, the factor of B is reduced from 0.0391 to 0.00021 at 50°C, The factor of N is reduced from 8.41E-05 to 4.68E-06 at 50°C.

C. COMPARED EXPERIMENT

In order to further verify the accuracy of the algorithm proposed in this paper, a set of comparative experiments is added. The MEMS gyroscope is kept on the temperature controlled oven in order to output the signal of MEMS gyroscopes and not influenced by outside temperature and humidity variation, then the ranges of temperature and temperature rate is set from 20°C to 60°C and 0.1°C/min. Firstly, the initial temperature and relative humidity should be set at 20°C and 50%RH then keep the temperature and relative humidity for an hour in order to make sure that the inside factors are stabled. Secondly, the temperature is raised at the rate of 0.1°C/min and keep the relative humidity as 50%RH. Next, the temperature controlled oven should be stay at each 10°C for an hour until 60°C in order to collect the output of MEMS gyroscope. Finally, repeat the above process and set the relative humidity of 60%RH, 70%RH, 80%RH, 90%RH. The process of compared experiment is shown in Figure 19, and the output of MEMS gyroscope is shown in Figure 20.

According to the IAWTD-CSVM-EEMD method proposed in this paper, the original signal of the MEMS gyroscope is firstly filtered by the IAWTD method, and the relative humidity drift of the original signal is obtained as shown in Figure 21.

Then the relative humidity drift, the relative humidity and the temperature change rate are used as input to establish the relative humidity model based on the C-SVM method In Figure 22, the accuracy of the relative humidity models established by C-SVM, SVM and RBF are compared, the humidity model established by the C-SVM method can better track the real output of relative humidity.

It can be described from Figure 23 that by using EEMD method, the output of the MEMS gyroscope becomes more

stable, the curve becomes smoother, and the relative humidity error is decreased a lot compared with KF, EKF and EMD. In order to further verify the compensation effect of IAWTD-C-SVM-EEMD, the results are compared it with IAWTD-RBF, GA-BP and CEEMDAN-ELM, the comparison results are given in Figure 24, and it can be seen that IAWTD-C-SVM-EEMD has the best effect. Finally, the Allan variance curve of the original signal and IAWTD-CSVM-EEMD method is shown in Figure 25, and the factors of Q, B, N based original data and IAWTD-CSVM-EEMD method are shown in Table 4.

V. CONCLUSION

The detailed relative humidity error of the MEMS gyroscope was studied based on a proposed new method named IAWTD-CSVM-EEMD. Within the improved fusion method based on full relative humidity experiment and compared experiment, the output of MEMS gyroscope has gone through a process of searching for humidity error, establishing humidity error compensation model, and filtering. The main findings are as follows:

(1) The new improved method IAWTD-CSVM-EEMD combined wavelet threshold denoising, C-SVM, and EMD related algorithms. The final output of the MEMS gyroscope decreased a lot compared to that of the Allan variance method, which indicated the good feasibility and effectiveness of the algorithms based on the novel method.

(2) By using the IAWTD-CSVM-EEMD method, the outputs of MEMS gyroscope, with the relative humidity ranged from 40% to 90% based on the temperature between 20 °C and 60 °C, reduced obviously. Under the temperature of 20 °C, 30 °C, 40 °C, 50 °C, and 60 °C, the drop rates of Q are 87.78%, 96.37%, 97.77%, 99.17%, 92.62%, respectively, the drop rates of B are 96.9%, 99.41%, 99.1%, 99.46%, 99.78%, respectively, and the drop rates of N are 88.16%, 96.54%, 98.16%, 94.43%, 92.05%, respectively.

(3) The improved method was also applicative to other conditions through the verification by a compared experiment with the temperature ranging from 20 °C to 60 °C based on the relative humidity from 50% to 90%. Under the conditions of 50RH%, 60RH%, 70RH%, 80RH%, and 90RH%, the drop rates of Q are 85.72%, 88.85%, 75.70%, 95.03%, 83.47%, respectively, the drop rates of B are 82.78%, 89.88%, 75.36%, 94.56%, 81.81%, respectively, and the drop rates of N are 88.16%, 96.54%, 98.16%, 94.43%, 92.05%, respectively.

REFERENCES

[1] D. Xia, C. Yu, and L. Kong, "The development of micromachined gyroscope structure and circuitry technology," *Sensors*, vol. 14, no. 1, pp. 1394–1473, Jan. 2014.
[2] T. Ma, Z. Li, H. Cao, C. Shen, and Z. Wang, "A parallel denoising model for dual-mass MEMS gyroscope based on PE-ITD and SA-ELM," *IEEE Access*, vol. 7, pp. 169979–169991, 2019.
[3] H. Gu, X. Liu, B. Zhao, and H. Zhou, "The in-operation drift compensation of MEMS gyroscope based on bagging-ELM and improved CEEMDAN," *IEEE Sensors J.*, vol. 19, no. 13, pp. 5070–5077, Jul. 2019.
[4] M. Wang, X. Dong, C. Qin, and J. Liu, "Adaptive H_∞ Kalman filter based random drift modeling and compensation method for ring laser gyroscope," *Measurement*, vol. 167, Jan. 2021, Art. no. 108170.
[5] D. Li, J. Zhou, and Y. Liu, "Recurrent-neural-network-based unscented Kalman filter for estimating and compensating the random drift of MEMS gyroscopes in real time," *Mech. Syst. Signal Process.*, vol. 147, Jan. 2021, Art. no. 107057.
[6] N. Song, Z. Yuan, and X. Pan, "Adaptive Kalman filter based on random-weighting estimation for denoising the fiber-optic gyroscope drift signal," *Appl. Opt.*, vol. 58, no. 35, p. 9505, Dec. 2019.
[7] J. Song, Z. Shi, B. Du, L. Han, H. Wang, and Z. Wang, "MEMS gyroscope wavelet de-noising method based on redundancy and sparse representation," *Microelectronic Eng.*, vol. 217, Sep. 2019, Art. no. 111112.
[8] D. Shu-Wen, L. Lu-Jun, W. Qing-Qu, W. Kang-Le, and C. Peng-Zhan, "Fiber optic gyro noise reduction based on hybrid CEEMDAN-LWT method," *Measurement*, vol. 161, Sep. 2020, Art. no. 107865.
[9] H. Xing, B. Hou, Z. Lin, and M. Guo, "Modeling and compensation of random drift of MEMS gyroscopes based on least squares support vector machine optimized by chaotic particle swarm optimization," *Sensors*, vol. 17, no. 10, p. 2335, Oct. 2017.
[10] J. Fei and Y. Yang, "Robust neural network control of MEMS gyroscope using adaptive sliding mode compensator," *Robotica*, vol. 34, no. 3, pp. 497–512, Mar. 2016.
[11] Z. Wang, J. Zhou, W. Du, Y. Lei, and J. Wang, "Bearing fault diagnosis method based on adaptive maximum cyclostationarity blind deconvolution," *Mech. Syst. Signal Process.*, vol. 162, Jan. 2022, Art. no. 108018, doi: 10.1016/j.ymssp.2021.108018.
[12] Z. Wang *et al.*, "A new fault diagnosis method based on adaptive spectrum mode extraction," *Struct. Health Monit.*, Jan. 2021, Art. no. 147592172098694, doi: 10.1177/1475921720986945.
[13] Z. Wang *et al.*, "Data-driven fault diagnosis method based on the conversion of erosion operation signals into images and convolutional neural network," *Process Saf. Environ. Protection*, vol. 149, no. 12, 2021.
[14] Y. Song, K. Zhao, X. Yan, and C. Li, "The adhesion failure in the MEMS accelerator influenced by relative humudity," *Chin. J. Sens. Actuators*, vol. 27, no. 3, pp. 316–319, 2014.
[15] T. Aono, K. Suzuki, M. Kanamaru, R. Okada, D. Maeda, M. Hayashi, and Y. Isono, "Development of wafer-level-packaging technology for simultaneous sealing of accelerometer and gyroscope under different pressures," *J. Micromech. Microeng.*, vol. 26, no. 10, Oct. 2016, Art. no. 105007.
[16] J. Makkonen, M. Broas, J. Li, J. Hokka, T. T. Mattila, and M. Paulasto-Krockel, "Reliability assessment of MEMS devices—A case study of a 3 axis gyroscope," in *Proc. 4th Electron. System-Integr. Technol. Conf.*, Sep. 2012, pp. 1–8.
[17] C. Patel and P. Mccluskey, "Performance degradation of the MEMS vibratory gyroscope in harsh environments," in *Proc. ASME Int. Mech. Eng. Congr. Expo.*, 2011, pp. 511–515.
[18] H. Cao, R. Cui, W. Liu, T. Ma, Z. Zhang, C. Shen, and Y. Shi, "Dual mass MEMS gyroscope temperature drift compensation based on TFPF-MEA-BP algorithm," *Sensor Rev.*, vol. 41, no. 2, pp. 162–175, May 2021, doi: 10.1108/SR-09-2020-0205.
[19] X. Chen and B. Cui, "Efficient modeling of fiber optic gyroscope drift using improved EEMD and extreme learning machine," *Signal Process.*, vol. 128, pp. 1–7, Nov. 2016.
[20] C. Liu, Z. Yang, Z. Shi, J. Ma, and J. Cao, "A gyroscope signal denoising method based on empirical mode decomposition and signal reconstruction," *Sensors*, vol. 19, no. 23, p. 5064, Nov. 2019.
[21] H. Cao, Z. Zhang, Y. Zheng, H. Guo, R. Zhao, Y. Shi, and X. Chou, "A new joint denoising algorithm for high-G calibration of MEMS accelerometer based on VMD-PE-wavelet threshold," *Shock Vib.*, vol. 2021, Jan. 2021, Art. no. 8855878, doi: 10.1155/2021/8855878.
[22] C. Shen, J. Li, X. Zhang, J. Tang, H. Cao, and J. Liu, "Multi-scale parallel temperature error processing for dual-mass MEMS gyroscope," *Sens. Actuators A, Phys.*, vol. 245, pp. 160–168, Jul. 2016.
[23] Y.-H. Tu and C.-C. Peng, "An ARMA-based digital twin for MEMS gyroscope drift dynamics modeling and real-time compensation," *IEEE Sensors J.*, vol. 21, no. 3, pp. 2712–2724, Feb. 2021.
[24] T. Yin, Y. Lin, H. Yang, and H. Wu, "A phase self-correction method for bias temperature drift suppression of MEMS gyroscopes," *J. Circuits, Syst. Comput.*, vol. 29, no. 12, Sep. 2020, Art. no. 2050198.
[25] L. Chang, H. Cao, and C. Shen, "Dual-mass MEMS gyroscope parallel denoising and temperature compensation processing based on WLMP and CS-SVR," *Micromachines*, vol. 11, no. 6, p. 586, Jun. 2020.

[26] R. Prasad, R. C. Deo, Y. Li, and T. Maraseni, "Soil moisture forecasting by a hybrid machine learning technique: ELM integrated with ensemble empirical mode decomposition," *Geoderma*, vol. 330, pp. 136–161, Nov. 2018.
[27] C. Shen, Y. Zhang, J. Tang, H. Cao, and J. Liu, "Dual-optimization for a MEMS-INS/GPS system during GPS outages based on the cubature Kalman filter and neural networks," *Mech. Syst. Signal Process.*, vol. 133, Nov. 2019, Art. no. 106222.

HUILIANG CAO (Member, IEEE) received the Ph.D. degree in instrument science and technology from Southeast University, Nanjing, China, in 2014. From 2011 to 2012, he studied as a Research Ph.D. Student with the School of Electrical and Computer Engineering, Georgia Institute of Technology, Atlanta, USA. He is currently a Postgraduate Tutor and an Associate Professor with the School of Instrument and Electronics, North University of China, Taiyuan, Shanxi, China. His research interest includes MEMS inertial devices. He is one of the Top Young Academic Leaders of Higher Learning Institutions of Shanxi and the Young Academic Leaders of the North University of China.

YUPENG LIU is currently pursuing the bachelor's degree with the School of Instrument and Electronics, North University of China, Taiyuan, Shanxi, China. His interest includes MEMS inertial devices.

LI LIU received the Ph.D. degree in instrument science and technology from Army Engineering University, Shijiazhuang, China, in 2018. She is currently a Lecturer with The Army Infantry Academy of PLA, Shijiazhuang. Her research interests include sensor and equipment development.

XINWANG WANG received the M.S. degree from the North University of China, Shanxi, China, in 2018. He is currently pursuing the Ph.D. degree with Southeast University, Nanjing, China. His research interests include navigation and guidance, structure and circuit of micro-machined gyroscope, artificial intelligence, and machine learning algorithm.